



HHS Public Access

Author manuscript

Angew Chem Int Ed Engl. Author manuscript; available in PMC 2015 June 30.

Published in final edited form as:

Angew Chem Int Ed Engl. 2012 December 14; 51(51): 12721–12726. doi:10.1002/anie.201205271.

Aptamer-Functionalized, Ultra-Small, Monodisperse Silica Nanoconjugates for Targeted Dual-Mode Imaging of Lymph Nodes with Metastatic Tumors**

Li Tang,

Department of Materials Science and Engineering, University of Illinois at Urbana-Champaign, 1304 W. Green Street, Urbana, IL, 61801 (USA)

Dr. Xujuan Yang,

Department of Food Science and Human Nutrition, University of Illinois at Urbana-Champaign

Prof. Dr. Lawrence W. Dobrucki,

Department of Bioengineering, University of Illinois at Urbana-Champaign

Isthier Chaudhury,

Department of Materials Science and Engineering, University of Illinois at Urbana-Champaign, 1304 W. Green Street, Urbana, IL, 61801 (USA)

Qian Yin,

Department of Materials Science and Engineering, University of Illinois at Urbana-Champaign, 1304 W. Green Street, Urbana, IL, 61801 (USA)

Catherine Yao,

Department of Materials Science and Engineering, University of Illinois at Urbana-Champaign, 1304 W. Green Street, Urbana, IL, 61801 (USA)

Prof. Dr. Stéphane Lezmi,

Department of Pathobiology, University of Illinois at Urbana-Champaign

Prof. Dr. William G. Helderich,

Department of Food Science and Human Nutrition, University of Illinois at Urbana-Champaign

Prof. Dr. Timothy M. Fan, and

Department of Veterinary Clinical Medicine, University of Illinois at Urbana-Champaign

Prof. Dr. Jianjun Cheng

Department of Materials Science and Engineering, University of Illinois at Urbana-Champaign, 1304 W. Green Street, Urbana, IL, 61801 (USA)

William G. Helderich: [helderic@illinois.edu](mailto:helderich@illinois.edu); Timothy M. Fan: t-fan@illinois.edu; Jianjun Cheng: jianjunc@illinois.edu

** J.C. acknowledges support from the NIH (Director's New Innovator Award 1DP2OD007246-01 and 1R21CA152627). L.T. was funded at University of Illinois at Urbana-Champaign from NIH National Cancer Institute Alliance for Nanotechnology in Cancer 'Midwest Cancer Nanotechnology Training Center' Grant R25 CA154015A.

Correspondence to: William G. Helderich, [helderic@illinois.edu](mailto:helderich@illinois.edu); Timothy M. Fan, t-fan@illinois.edu; Jianjun Cheng, jianjunc@illinois.edu.

Supporting information for this article is available on the WWW under <http://www.angewandte.org> or from the author.

Keywords

silica nanoparticle; nanoconjugate; dual-modal imaging; metastasis targeting; sentinel lymph node; aptamer; breast cancer

Metastases are responsible for 90% of human cancer deaths.^[1] Most solid tumors metastasize through the circulation system, and the sentinel lymph node (LN) is typically the first site reached by the disseminating malignant cancer cells.^[2] The detection of LN metastases is therefore crucial for accurate tumor staging and therapeutic decision-making.^[3] The current standard method for LN assessment is lymphography using a vital blue dye. However, this method is invasive, involving extended nodal dissection, and can give a false negative result if a LN is missed in surgery.^[4] A non-invasive LN imaging technique is urgently needed to improve the accuracy of tumor staging.^[5] Various techniques for sentinel LN imaging have been investigated, such as near-infrared (NIR) fluorescence imaging, computed tomography (CT), magnetic resonance imaging (MRI), positron emission tomography (PET), and ultrasound and photoacoustic imaging.^[4b, 5b, 6] However, each technique has its drawbacks, and none is sufficient to provide all the necessary information for LN assessment. ^[4b] PET is the most sensitive and specific technique for *in vivo* molecular imaging,^[7] but it suffers from low spatial resolution. In contrast, fluorescence imaging has high resolution and allows spatial visualization, which is helpful for intraoperative guidance; but its application is limited by poor tissue penetration. Therefore, combination of both PET and fluorescence imaging together potentially permit non-invasive assessment of LNs with high sensitivity and excellent spatial resolution.

Silica nanoparticles (NPs) are widely used for biomedical imaging applications because of the good biocompatibility and optically transparency of silica.^[8] We recently developed a versatile, size-controlled, monodisperse drug/dye–silica nanoconjugate (NC) platform that allows for conjugation with a variety of functional moieties.^[9] The robust silane chemistry and the formulation strategy permit the construction of multifunctional NCs, such as multimodal imaging probes for *in vivo* applications. It is generally accepted that the physicochemical properties of NPs, especially their size, play a vital role in the systemic and lymphatic biodistribution.^[10] Because the size of the silica NCs can be precisely controlled, they are ideal for investigating size effects on their trafficking behavior in the lymphatic system. The silica NCs provide a unique platform with multifunctionality and excellent size control for the preparation of nanoparticulate probes with optimized properties for improved imaging of LN metastases.^[10c]

There have been many studies on the targeting of primary tumors,^[11] but very few attempts have been made to actively target metastatic tumors specifically.^[12] As an alternative to antibodies for cancer targeting, aptamers (Apts), single-stranded oligonucleotides that can bind to target molecules with high specificity and affinity, have attracted much attention because they are small, easy to synthesize, non-immunogenic, and capable being engineered to resist denaturation and biodegradation.^[13] The capability of Apts to target primary tumors has been demonstrated in several studies *in vivo*.^[13b, 13c] However, active targeting of lymphatic metastases using Apts has not been reported.

Herein we report a convenient, one-pot synthesis of monodisperse, size-controlled silica NC probes for dual-modal LN imaging of PET and NIR fluorescence. Monodisperse 20-nm silica NCs accumulated in sentinel LNs more rapidly and to a greater extent than larger NCs (200 nm) and were superior for efficient LN imaging. To further enhance the targeting of LNs with metastatic tumors, we functionalized the 20-nm silica NCs with a 26-mer G-rich DNA Apt derived from AS1411, which has high binding affinity for nucleolin (NCL), a protein that is over-expressed in the cytoplasm and on the plasma membrane of some cancer cells, including breast cancer cells.^[14] The NCL-Apt-functionalized silica NCs showed markedly enhanced uptake in LNs with metastatic tumors in a murine breast tumor model, and improved the detection efficiency of metastatic tumors in LNs.

Silica NCs for dual-modal imaging were synthesized in a manner similar to that reported recently.^[9] We first synthesized a silane-modified NIR dye (NIR-sil) and a silanized chelating reagent (DOTA-sil) that can bind a radionuclide (*e.g.*, ⁶⁴Cu) for PET imaging. Because silica is optically transparent and the excitation and emission light can pass through the silica matrix, NIR-sil was added immediately after the addition of tetraethyl orthosilicate (TEOS) so that the NIR imaging ligand was stably bound to and homogeneously distributed in the silica NCs (Scheme 1).^[15] DOTA-sil was added to the NIR-dye-doped silica NCs for conjugation of DOTA to their surface for chelation of radionuclides. Poly(ethylene glycol)-containing silane (PEG-sil) was then used to graft PEG to the surface of the silica NCs. Surface PEGylation of NPs is routinely employed to prolong circulation, minimize nonspecific absorption, and reduce particle aggregation *in vivo*.^[16] Finally, the as-prepared PEGylated NCs were labeled with ⁶⁴Cu by means of a chelation reaction (Scheme 1, Figure S1).

We used the described procedure to prepare NIR- and DOTA-modified silica NCs with controlled sizes of 200 and 20 nm (denoted NC200 and NC20, respectively; Figure 1a). NC200 and NC20 showed strong fluorescence emission at λ_{em} values of 802.5 and 808.0 nm, respectively (Figure 1b).^[17] Effective surface modification with DOTA was evidenced by the ζ -potential measurement (Figure 1c). Both NC200 and NC20 had negatively charged surfaces (-34.8 and -36.3 mV, respectively; Figure 1c) at pH 7.4, owing to the surface-bound carboxyl groups of DOTA (Scheme 1). These NCs chelated ⁶⁴Cu cations ($t_{1/2} = 12.7$ h, $\beta^+ = 17.4\%$) with high labeling efficiency (>60%, Figures 1c and S1) and good labeling stability in 50% reconstituted human serum (mimicking physiological conditions; Figure S2).

As expected, the size of the as-prepared dual-modal silica NCs was well controlled.^[9] Scanning electron microscopy (SEM) indicated that the diameters of NC200 and NC20 were 198.7 ± 11.8 and 23.1 ± 2.3 nm, respectively (Figure 1a, c). Remarkably narrow size distributions with coefficients of variation (CV) <10% were observed for both NCs. Thus, these silica NCs, which we designed to serve as a platform for preparing nanoparticulate multimodal imaging probes, feature synthetic convenience, flexibility, excellent size control, and modularity that allows for alteration of the functionality and surface chemistry.

To explore the use of the silica NCs for non-invasive PET/CT imaging of LNs *in vivo* and to identify the optimal NP size for the most efficient LN accumulation, we investigated the lymphatic trafficking of ⁶⁴Cu-labeled NC200 and NC20 in normal C57BL/6 mice (Figure

2a). Each mouse received small-volume interstitial injections (a commonly used administration route for lymphatic distribution studies)^[10f, 10g, 18] of the two NCs, one into each rear hock (left, NC20; right, NC200). PET imaging was carried out to monitor the distribution of the NCs on both sides (Figure 2b). The positions of popliteal LNs (P-LNs), which are the closest LNs to the injection sites, can be clearly identified in the CT images (yellow arrows, Figure 2b). The overlaid CT and PET images show noticeable radioactivity in the left P-LN as early as 12 min post injection (p.i.) but not in the right P-LN. The signal increased rapidly in the left P-LN from 3.5% I.D./g at 12 min p.i. to 9.8% I.D./g at 62 min p.i., suggesting fast and efficient lymphatic draining of NC20 (Figure 2d). The amount of accumulated NC20 in the left P-LN continued to increase slightly over time, eventually reaching a plateau at about 6 h p.i. (10.3% I.D./g). This high level of lymphatic accumulation was maintained for as long as 24 h p.i. (10.4% I.D./g), suggesting that NC20 were preferentially retained in the LNs, presumably because they were phagocytosed by resident nodal macrophages and dendritic cells.^[8a, 10f, 19] In contrast, the signal detected in the right P-LN, on the side that had been injected with NC200, was negligible during the first hour p.i. (0.66 and 1.9% I.D./g at 12 and 62 min p.i., respectively); the majority of the NC200 remained highly localized at the injection site. The radioactivity in the right P-LN remained low at 6 and 24 h p.i. (1.3 and 2.7% I.D./g, respectively). These observations suggest that NC20 gained entrance to and traveled more readily in the lymphatic system than their 200-nm counterparts. Three-dimensional reconstructed image and movie (Figure 2c, Movie S1) also provide evidence for the significantly enhanced accumulation of NC20 in the left P-LN at 6 h p.i. At 24 h p.i., accumulation of NC20 was ~3.8 times of that of NC200 (Figure 2d). These results were confirmed by *ex vivo* measurement of the radioactivity in the excised P-LNs with a γ -counter (0.50 and 0.13 μ Ci/g for NC20 and NC200, respectively; Figure 2e).

Because the silica NCs were also labeled with NIR dye, they have the potential to be useful for intraoperative guidance and high-resolution LN imaging. To demonstrate the use of the integrated NIR fluorophore for fluorescence imaging, we harvested the inguinal LNs (I-LNs) from both sides 24 h p.i. for *ex vivo* imaging with an Odyssey NIR imaging system (Figure 3a, b). A strong fluorescence signal (298.9 a.u.) was observed in the left I-LN where NC20 was injected into the ipsilateral hock; whereas a much weaker fluorescence signal (50.5 a.u.) was detected in the right I-LN after injection with NC200 (Figure 3c). The fluorescence enhancement of NC20 in the left I-LN indicates that NC20 migrated ~6 times as efficiently to distant regional LNs through the lymphatic vessels as did NC200.

The preferential accumulation of NC20 in both the P-LNs and the I-LNs demonstrates that NC20 was taken up by the lymphatic system much more rapidly and was retained in the LNs at higher levels and for a longer time than their larger counterparts. Because of the sustained LN accumulation, use of NC20 might overcome the problem with vital blue dyes (*e.g.*, Evans blue), which is that they diffuse away from the LNs too rapidly to allow prolonged imaging.^[4b, 10d] Clearly, the size of the nanoprobe played a vital role in controlling their lymphatic trafficking. NC20 diffused rapidly from the interstitial space into the lymphatic vessels, owing to their ultra-small size, and they efficiently migrated to the draining LNs once they reached the lymphatic vessels.^[10f, 20] NCs with diameters \leq 100 nm are likely to

be internalized by peripheral dendritic cells first and then taken to the LNs by these cells.^[10f, 20] This process usually takes more than 24 h, which could explain the small increase in LN accumulation of NC200 at 24 h p.i. (Figure 2d). Our observations agree with the recent reports by Wang *et al.*^[10g] and Reddy *et al.*^[10f] that 20–30 nm NPs are transported to LNs much more efficiently than 100-nm NPs after interstitial injection. The NP of 20 nm may also outperform the NPs of 30–50 nm with regard to lymphatic uptake.^[10a, 10e, 10f, 21] In contrast, NPs with sizes <8 nm may preferentially migrate to the blood circulation and be cleared rapidly *via* the renal system.^[10b, 10d] Thus, 20-nm silica NC is likely in the optimum size range (10–20 nm) for the most efficient passive targeting of LNs.

Next, we functionalized the surface of NC20 with NCL-Apt to assess the capability of Apt-functionalized NCs to target metastatic sentinel LNs. Scheme 1 illustrates the conjugation of NCL-Apt to the surface-bound PEG of silica NCs. Control DNA (Ctrl-DNA) with a random sequence was also conjugated to NC20 for comparison. The successful DNA conjugation was achieved with high conjugation efficiency (C.E.) (73.2 and 79.6% for Ctrl-DNA- and NCL-Apt-functionalized NC20s, respectively; designated as NC20-Ctrl and NC20-Apt; Figure 1c). The DNA surface densities of NC20-Ctrl and NC20-Apt were 8.6 and 9.4 DNA molecules per NC, respectively (Figure 1c).

To evaluate the targeting capability of NC20-Apt *in vitro*, we separately incubated Rhodamine B isothiocyanate (RITC)-labeled NC20-Ctrl and NC20-Apt with 4T1 murine breast cancer cells. Flow cytometry analysis showed that there was a 1.6-fold increase in mean fluorescence intensity in 4T1 cells treated with NC20-Apt (20.8 a.u.) versus cells treated with NC20-Ctrl (13.1 a.u.) (Figure 4a). Of the cells incubated with NC20-Apt for 2 h, 70.7% became fluorescently positive, whereas only 57.5% became positive after incubation with NC20-Ctrl (Figure S3). These results clearly demonstrate that NC20-Apt had enhanced ability to bind to 4T1 breast cancer cells *in vitro*.

Because NC20-Apt was selectively taken up by the 4T1 cancer cells, we expected that NC20-Apt would show enhanced accumulation in LNs with metastatic 4T1 tumors. Therefore, we evaluated the capability of NC20-Apt to target metastatic tumors in sentinel LNs *in vivo*. First, we established a LN metastasis tumor model by hock inoculation of 4T1 cells (stably transfected with firefly luciferase) in both legs of female BABL/c mice through interstitial injection.^[8a, 22] After 8 days, visible primary tumors had developed, and strong localized bioluminescent signals from 4T1 tumors were detected (Figure S4a). Tumor cells also metastasized to the P-LNs, as evidenced by their enlarged size and histological analysis of the excised metastatic P-LNs (mP-LNs, Figure S4b–d).^[12c, 23] Next, NC20-Ctrl and NC20-Apt were subcutaneously injected into the interstitial space between the primary tumors and the mP-LNs (left, NC20-Ctrl; right, NC20-Apt; Figure 4b) in a mouse with mP-LNs on both sides. We acquired PET/CT images 24 h p.i. to compare the uptake of both NCs in the mP-LNs. A much stronger PET signal was clearly observed in the right mP-LN, on the side injected with NC20-Apt (Figure 4c). The accumulation of NC20-Apt in the mP-LN was ~2.3 times of that of NC20-Ctrl, as indicated by quantification of the radioactivity in the PET images (6.2 and 14.6% I.D./g for NC20-Ctrl and NC20-Apt, respectively; Figure 4d). This result was also confirmed by *ex vivo* measurement of the radioactivity in the

excised mP-LNs with a γ -counter (6.5 and 14.8% I.D./g for NC20-Ctrl and NC20-Apt, respectively; Figure 4e), which correlates well with the *in vivo* data. On the other hand, each mouse with mP-LN on one side (right) and normal P-LN on the other (left) received interstitial injections of NC20-Apt into both rear hocks (Figure S5a). It is noticeable that there was a ~ 2.1 fold increase in NC20-Apt accumulation in the mP-LN compared to the normal P-LN (5.9 and 12.1% I.D./g for P-LN and mP-LN, respectively; Figure S5b).

The clearly increased accumulation of NC20-Apt in the mP-LNs was likely due to selective uptake by the metastatic 4T1 cells in the mP-LNs.^[12a] The enhanced uptake and retention of the Apt-functionalized dual-modal silica NCs in metastatic LNs permits discrimination of metastatic and normal LNs and thus improves the efficiency of tumor metastasis detection. A widely used conventional strategy for improving LN accumulation is surface decoration of NPs with sugar molecules to enhance uptake by macrophages, which home to LNs.^[24] However, macrophages that take up the sugar-modified NPs may also transport these NPs to the blood circulation, resulting in non-specific accumulation in other organs (*e.g.*, liver and spleen). Antibodies^[12b, 25] and peptides^[12a, 12c, 15a, 22] are also employed as active targeting ligands to modify the surface of NPs to improve the targeting efficiency for metastatic tumors in LNs. However, the application of antibodies or peptides is limited by their relatively instability, high cost, and difficult large-scale preparation. Highly specific Apt-functionalized silica NC imaging probes may overcome these limitations and have potential applications in clinical settings.

In conclusion, we developed monodisperse, size-controlled silica NCs for dual-modal PET/NIR imaging of sentinel LNs. Dual-modal imaging using this novel probe has unique advantages over conventional lymphatic imaging techniques. For example, PET imaging is a noninvasive diagnostic method and overcomes the depth-insensitivity of optical imaging tools, and NIR fluorescence imaging can compensate for the relatively low spatial resolution of PET imaging and potentially provide convenient intraoperative guidance for resection of metastatic LNs once they are identified. When the size of the silica NCs was controlled to as small as 20 nm, they accumulated rapidly and effectively in LNs, thus allowing for improved LN imaging *in vivo*. For the first time, Apt was utilized to functionalize silica NCs for active targeting of lymphatic metastases. Uptake and retention of the Apt-functionalized silica NCs in metastatic LNs were significantly enhanced compared to the non-targeted silica NCs. These dual labeled silica NCs hold great potential for improving the accuracy of clinical tumor staging by serving as probes for efficient noninvasive targeted imaging of metastatic LNs.

Supplementary Material

Refer to Web version on PubMed Central for supplementary material.

References

1. Chaffer CL, Weinberg RA. *Science*. 2011; 331:1559–1564. [PubMed: 21436443]
2. Tammela T, Saaristo A, Holopainen T, Ylä-Herttua S, Andersson LC, Virolainen S, Immonen I, Alitalo K. *Sci Transl Med*. 2011; 3:69ra11.

3. a) Aikou T, Kitagawa Y, Kitajima M, Uenosono Y, Bilchik AJ, Martinez SR, Saha S. *Cancer Metastasis Rev.* 2006; 25:269–277. [PubMed: 16770539] b) Harisinghani MG, Barentsz J, Hahn PF, Deserno WM, Tabatabaei S, van de Kaa CH, de la Rosette J, Weissleder R. *N Engl J Med.* 2003; 348:2491–2499. [PubMed: 12815134]
4. a) Lucarelli RT, Ogawa M, Kosaka N, Turkbey B, Kobayashi H, Choyke PL. *Lymphat Res Biol.* 2009; 7:205–214. [PubMed: 20143919] b) Zhang F, Niu G, Lu GM, Chen XY. *Mol Imaging Biol.* 2011; 13:599–612. [PubMed: 20862613]
5. a) Nune SK, Gunda P, Majeti BK, Thallapally PK, Forrest ML. *Adv Drug Deliv Rev.* 2011; 63:876–885. [PubMed: 21718728] b) Cohen SM, Fishinghawk BG, Cohen MS. *Adv Drug Deliv Rev.* 2011; 63:956–962. [PubMed: 21683745]
6. Moghimi SM, Bonnemain B. *Adv Drug Deliv Rev.* 1999; 37:295–312. [PubMed: 10837741]
7. Sun Y, Yu MX, Liang S, Zhang YJ, Li CG, Mou TT, Yang WJ, Zhang XZ, Li BA, Huang CH, Li FY. *Biomaterials.* 2011; 32:2999–3007. [PubMed: 21295345]
8. a) Huang XL, Zhang F, Lee S, Swierczewska M, Kiesewetter DO, Lang LX, Zhang GF, Zhu L, Gao HK, Choi HS, Niu G, Chen XY. *Biomaterials.* 2012; 33:4370–4378. [PubMed: 22425023] b) Benezra M, Penate-Medina O, Zanzonico PB, Schaer D, Ow H, Burns A, DeStanchina E, Longo V, Herz E, Iyer S, Wolchok J, Larson SM, Wiesner U, Bradbury MS. *J Clin Invest.* 2011; 121:2768–2780. [PubMed: 21670497] c) Kumar R, Roy I, Ohulchanskyy TY, Vathy LA, Bergoy EJ, Sajjad M, Prasad PN. *ACS Nano.* 2010; 4:699–708. [PubMed: 20088598] d) Wang L, Wang KM, Santra S, Zhao XJ, Hilliard LR, Smith JE, Wu JR, Tan WH. *Anal Chem.* 2006; 78:646–654. e) Rieter WJ, Kim JS, Taylor KML, An HY, Lin WL, Tarrant T, Lin WB. *Angew Chem.* 2007; 119:3754–3756. *Angew Chem, Int Ed.* 2007; 46:3680–3682. f) Meng H, Xue M, Xia T, Ji Z, Tarn DY, Zink JJ, Nel AE. *ACS Nano.* 2011; 5:4131–4144. [PubMed: 21524062]
9. Tang L, Fan TM, Borst LB, Cheng J. *ACS Nano.* 2012; 6:3954–3966. [PubMed: 22494403]
10. a) Cai X, Li W, Kim CH, Yuan Y, Wang LV, Xia Y. *ACS Nano.* 2011 b) Kaminskas LM, Porter CJH. *Adv Drug Deliv Rev.* 2011; 63:890–900. [PubMed: 21683746] c) Oussoren C, Storm G. *Adv Drug Deliv Rev.* 2001; 50:143–156. [PubMed: 11489337] d) Kobayashi H, Kawamoto S, Bernardo M, Brechbiel MW, Knopp MV, Choyke PL. *J Controlled Release.* 2006; 111:343–351. e) Reddy ST, Rehor A, Schmoekel HG, Hubbell JA, Swartz MA. *J Controlled Release.* 2006; 112:26–34. f) Reddy ST, van der Vlies AJ, Simeoni E, Angeli V, Randolph GJ, O'Neil CP, Lee LK, Swartz MA, Hubbell JA. *Nat Biotechnol.* 2007; 25:1159–1164. [PubMed: 17873867] g) Wang H, Wang ST, Su H, Chen KJ, Armijo AL, Lin WY, Wang YJ, Sun J, Kamei K, Czernin J, Radu CG, Tseng HR. *Angew Chem.* 2009; 121:4408–4412. *Angew Chem, Int Ed.* 2009; 48:4344–4348. h) Goodman TT, Olive PL, Pun SH. *Int J Nanomedicine.* 2007; 2:265–274. [PubMed: 17722554] i) Perrault SD, Walkey C, Jennings T, Fischer HC, Chan WCW. *Nano Lett.* 2009; 9:1909–1915. [PubMed: 19344179]
11. a) Peer D, Karp JM, Hong S, Farokhzad OC, Margalit R, Langer R. *Nat Nanotechnol.* 2007; 2:751–760. [PubMed: 18654426] b) Davis ME, Chen Z, Shin DM. *Nat Rev Drug Discov.* 2008; 7:771–782. [PubMed: 18758474]
12. a) Leuschner C, Kumar C, Hansel W, Soboyejo W, Zhou JK, Hormes J. *Breast Cancer Res Treat.* 2006; 99:163–176. [PubMed: 16752077] b) Sampath L, Kwon S, Hall MA, Price RE, Sevcik-Muraca EM. *Transl Oncol.* 2010; 3:307–317. [PubMed: 20885893] c) Yan ZQ, Zhan CY, Wen ZY, Feng LL, Wang F, Liu Y, Yang XK, Dong Q, Liu M, Lu WY. *Nanotechnology.* 2011; 22
13. a) Shangguan D, Li Y, Tang ZW, Cao ZHC, Chen HW, Mallikaratchy P, Sefah K, Yang CYJ, Tan WH. *Proc Natl Acad Sci.* 2006; 103:11838–11843. [PubMed: 16873550] b) Cheng J, Teply BA, Sherifi I, Sung J, Luther G, Gu FX, Levy-Nissenbaum E, Radovic-Moreno AF, Langer R, Farokhzad OC. *Biomaterials.* 2007; 28:869–876. [PubMed: 17055572] c) Farokhzad OC, Cheng J, Teply BA, Sherifi I, Jon S, Kantoff PW, Richie JP, Langer R. *Proc Natl Acad Sci.* 2006; 103:6315–6320. [PubMed: 16606824]
14. a) Cao Z, Tong R, Mishra A, Xu W, Wong GCL, Cheng J, Lu Y. *Angew Chem.* 2009; 121:6616–6620. *Angew Chem, Int Ed.* 2009; 48:6494–6498. b) Christian S, Pilch J, Akerman ME, Porkka K, Laakkonen P, Ruoslahti E. *J Cell Biol.* 2003; 163:871–878. [PubMed: 14638862] c) Soundararajan S, Chen WW, Spicer EK, Courtenay-Luck N, Fernandes DJ. *Cancer Res.* 2008; 68:2358–2365. [PubMed: 18381443]

15. a) Benezra M, Penate-Medina O, Zanzonico PB, Schaer D, Ow H, Burns A, DeStanchina E, Longo V, Herz E, Iyer S, Wolchok J, Larson SM, Wiesner U, Bradbury MS. *J Clin Invest*. 2011; 121:2768–2780. [PubMed: 21670497] b) Ha SW, Camalier CE, Beck GR, Lee JK. *Chem Commun*. 2009:2881–2883.
16. Caliceti P, Veronese FM. *Adv Drug Deliv Rev*. 2003; 55:1261–1277. [PubMed: 14499706]
17. Narayanan N, Patonay G. *J Org Chem*. 1995; 60:2391–2395.
18. Chaney EJ, Tang L, Tong R, Cheng JJ, Boppart SA. *Mol Imaging*. 2010; 9:153–162. [PubMed: 20487681]
19. Alex JC, Weaver DL, Fairbank JT, Rankin BS, Krag DN. *Surg Oncol*. 1993; 2:303–308. [PubMed: 8305972]
20. Bachmann MF, Jennings GT. *Nat Rev Immunol*. 2010; 10:787–796. [PubMed: 20948547]
21. Moghimi SM, Hunter AC, Murray JC. *FASEB J*. 2005; 19:311–330. [PubMed: 15746175]
22. Zhang F, Niu G, Lin X, Jacobson O, Ma Y, Eden H, He Y, Lu G, Chen X. *Amino Acids*. 2012; 42:2343–2351. [PubMed: 21769497]
23. Yan ZQ, Wang F, Wen ZY, Zhan CY, Feng LL, Liu Y, Wei XL, Xie C, Lu WY. *J Controlled Release*. 2012; 157:118–125.
24. a) Hieu VQ, Yoo MK, Jeong HJ, Lee HJ, Muthiah M, Rhee JH, Lee JH, Cho CS, Jeong YY, Park IK. *Acta Biomater*. 2011; 7:3935–3945. [PubMed: 21763797] b) Ocampo-Garcia BE, Ramirez FD, Ferro-Flores G, De Leon-Rodriguez LM, Santos-Cuevas CL, Morales-Avila E, de Murphy CA, Pedraza-Lopez M, Medina LA, Camacho-Lopez MA. *Nucl Med Biol*. 2011; 38:1–11. [PubMed: 21220124]
25. Takeda M, Tada H, Higuchi H, Kobayashi Y, Kobayashi M, Sakurai Y, Ishida T, Ohuchi N. *Breast Cancer*. 2008; 15:145–152. [PubMed: 18317884]

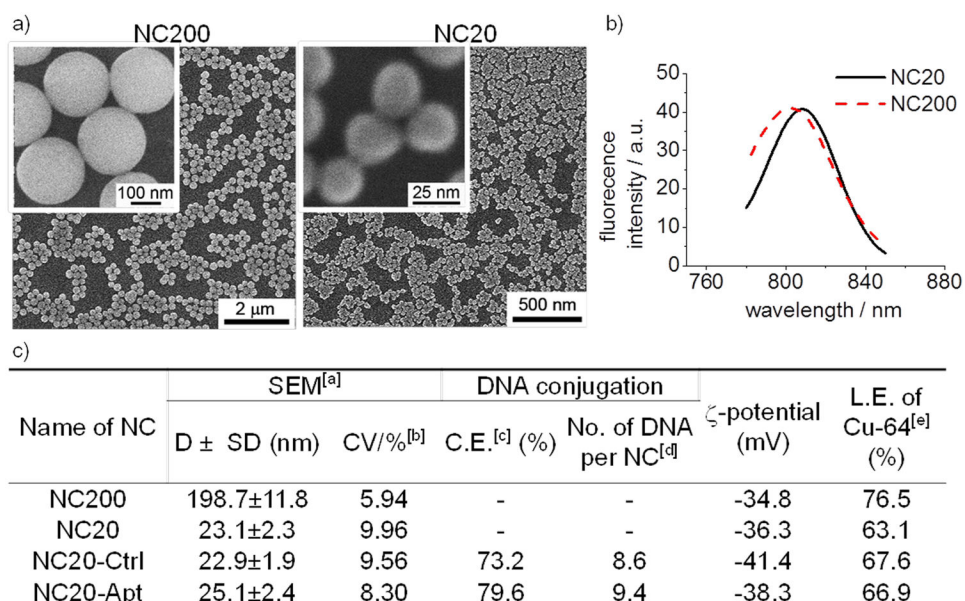


Figure 1.

a) SEM images of silica NCs show excellent size control. b) Fluorescence emission spectrum of dual labeled silica NCs. c) The characterizations of silica NCs. ([a] The sizes of the hard cores were measured by SEM. D= average diameter, SD=standard deviation. [b] CV=SD/D. [c] The conjugation efficiencies (C.E.) of Ctrl- and Apt-DNA were determined by quantifying the DNA concentration in the supernatant with a Nanodrop spectrophotometer after the NCs were centrifuged down. [d] The number (No.) of DNA molecules per NC was calculated from the DNA/NC feeding ratio and the C.E. value. The silica NC density was set at 2.56 g/cm³. [e] The ⁶⁴Cu labeling efficiency (L.E.) was determined by quantifying the radioactivity in the supernatant with a γ -counter).

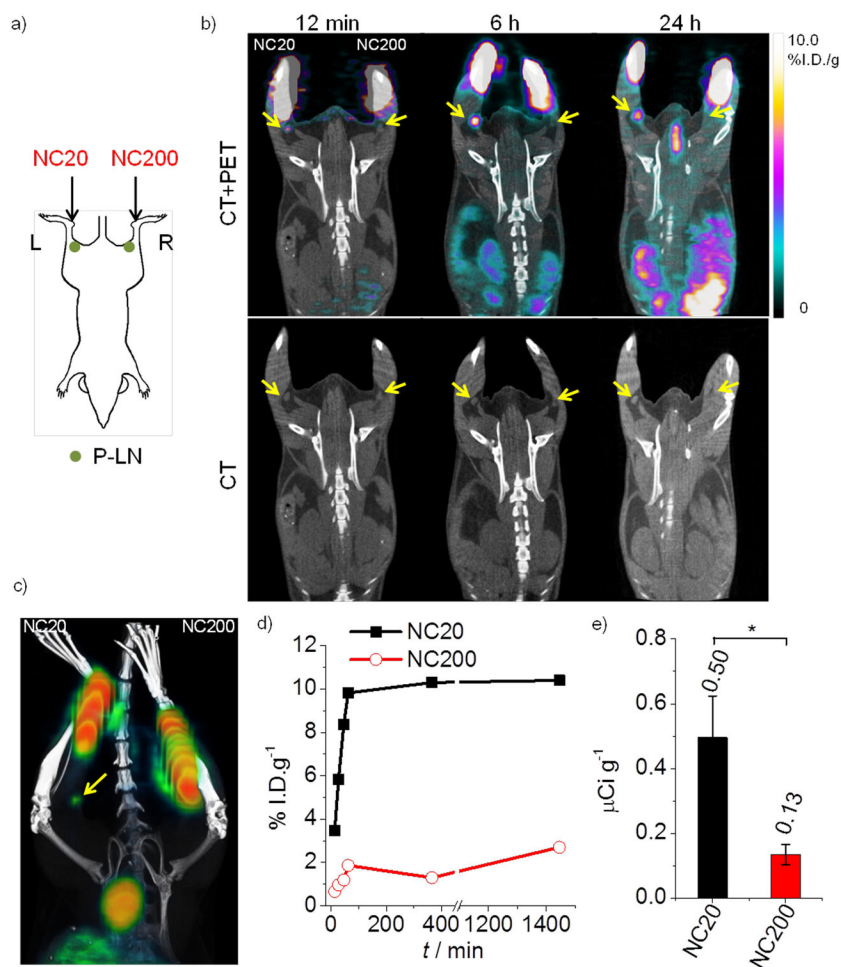


Figure 2.

a) Dual labeled NC20 (left) and NC200 (right) were administered to normal C57BL/6 mice by hock injection; the same amount of radioactivity was injected on each side. b) *In vivo* whole-body dynamic PET/CT imaging of mice was performed to assess the accumulation of the silica NCs in the P-LNs (yellow arrows in coronal views). c) A corresponding three-dimensional PET/CT image at 6 h p.i. shows enhanced accumulation of NC20 in the left P-LN (yellow arrows). d) The kinetics of the accumulation of ^{64}Cu -labeled NCs in the P-LNs was quantified by selecting the regions of interest in the PET images and analyzing with the instrument software. e) The radioactivity in the excised P-LNs (24 h p.i.) was measured *ex vivo* with a γ -counter (average \pm SD; $n = 3$; $*p < 0.05$).

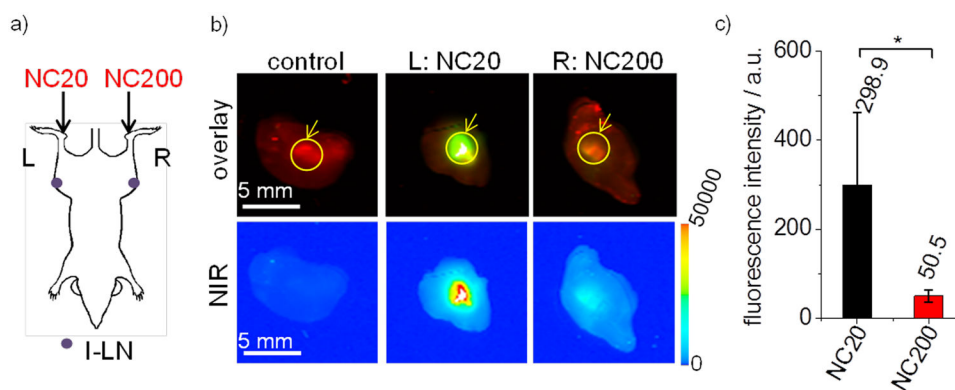


Figure 3.

a) Dual labeled NC20 (left) and NC200 (right) were administered to normal C57BL/6 mice by hock injection. b) I-LNs were collected and imaged for NIR fluorescence at $\lambda_{em} = 800$ nm (green) and autofluorescence from tissues (including the surrounding fat) at $\lambda_{em} = 700$ nm (red). The overlaid images of these two channels are shown in the first row. The I-LNs are indicated by yellow circles and arrows. The second row shows the pseudo-colored images of the NIR fluorescence intensity in the I-LNs. c) The NIR fluorescence intensity in each I-LN was measured *ex vivo* at $\lambda_{em} = 800$ nm with an Odyssey NIR imaging system (average \pm SD; $n = 3$; $*p < 0.05$).

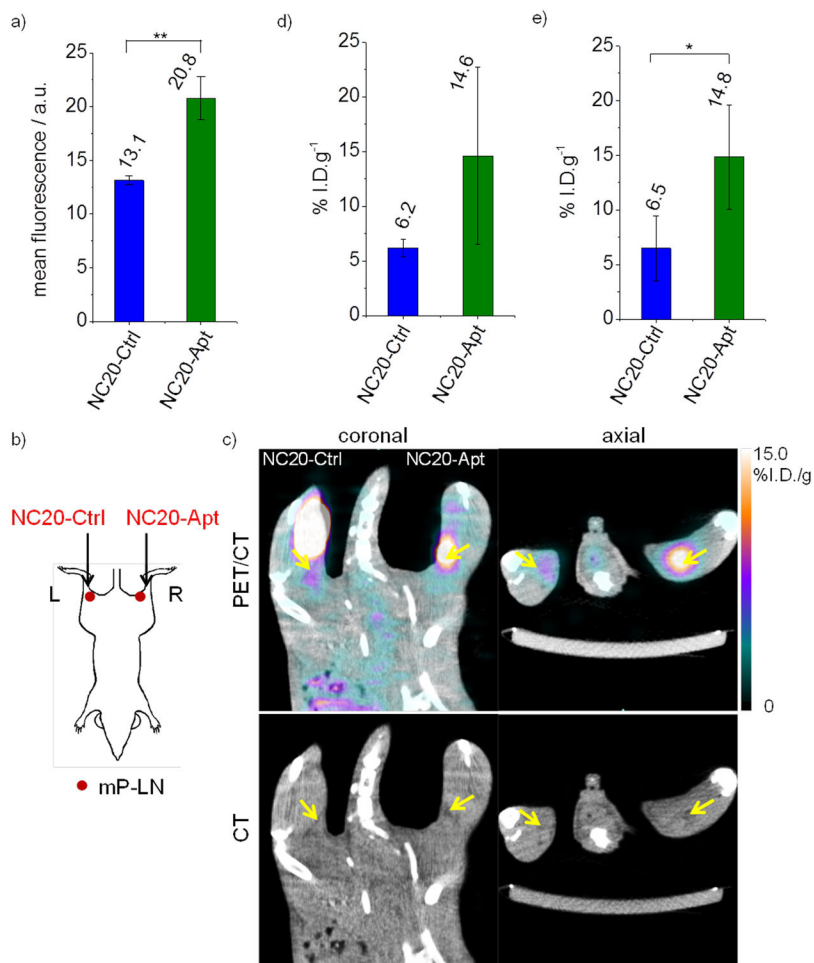
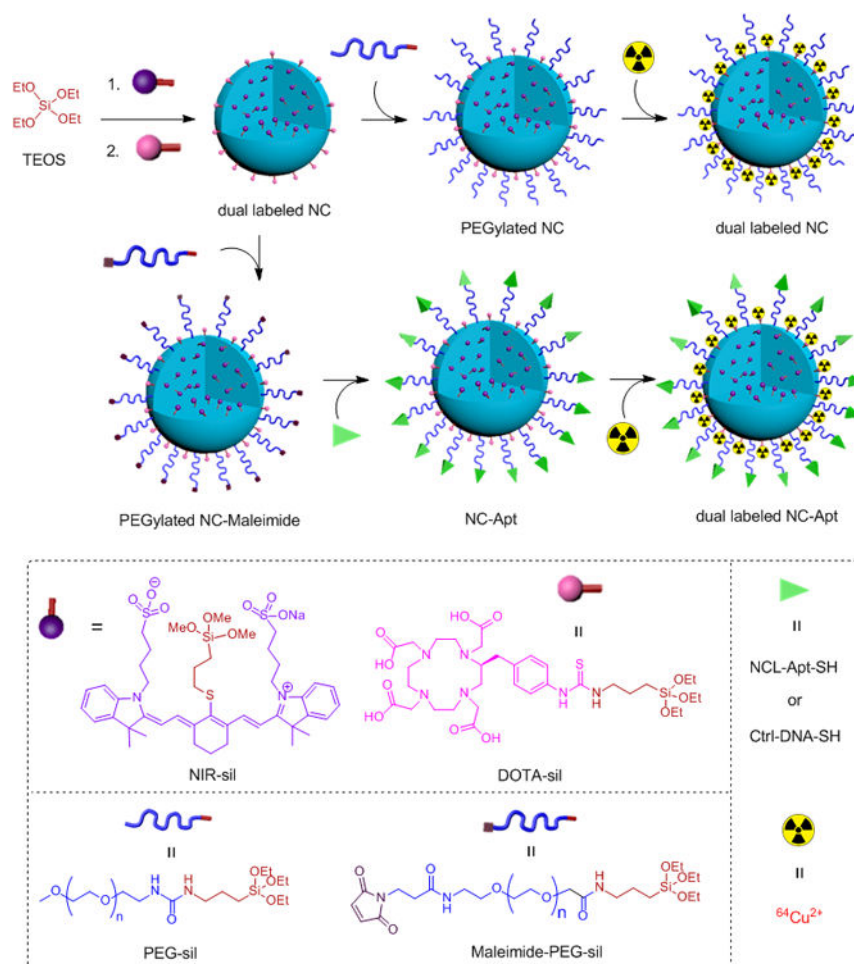


Figure 4.

a) *In vitro* 4T1 cell targeting with NC20-Apt. Internalization of NC20-Ctrl and NC20-Apt by 4T1 cells over 2 h incubation at 37 °C was evaluated from the mean fluorescence of treated cells measured using flow cytometry. b) Dual labeled NC20-Ctrl (left) and NC20-Apt (right) were administered to BALB/c mice with metastatic LNs by hock injection. c) *In vivo* whole-body PET/CT imaging of BALB/c mice was performed at 24 h p.i. to assess the accumulation of silica NCs in mP-LNs (yellow arrows in coronal and axial views). d) Accumulation of the ^{64}Cu -labeled NCs in the mP-LNs was quantified by selecting the regions of interest in the PET images and analyzing with the instrument software. e) Accumulation of the ^{64}Cu -labeled NCs was confirmed by *ex vivo* measurement of excised mP-LNs with a γ -counter (average \pm SD; $n = 3$; $*p < 0.05$).



Scheme 1. Preparation of aptamer-functionalized dual-modal silica NCs for both PET and NIR fluorescence imaging.